

Article

Refinement of Norrbin Model via Correlations between Dimensionless Cross-Flow Coefficient and Hydrodynamic Derivatives

Guoshuai Li, Yifan Chen, Bingzheng Yan and Xianku Zhang * 

Navigation College, Dalian Maritime University, Dalian 116023, China; liguoshuai@dlnu.edu.cn (G.L.); artoriacl@163.com (Y.C.); dmuybz@163.com (B.Y.)

* Correspondence: zhangxk@dlnu.edu.cn

Abstract: To develop a simplified and highly accurate ship motion model, this study thoroughly investigated the relationship between the dimensionless cross-flow coefficient and the four hydrodynamic derivatives of the Norrbin model. Eight different types of ships were simulated to explore the impact of dimensionless cross-flow coefficients and individual hydrodynamic derivatives on the ship's turning circle. A set of precise formulas is proposed to depict the interplay between these variables. The simulation outcomes indicate that the average deviation in the agreement between the turning circles produced by adjusting the dimensionless cross-flow coefficient and those predicted by modifying the four hydrodynamic derivatives was only 2.70%. Furthermore, the similarities between the two circles and the sea trail were significantly higher at 91.45% and 92.87% compared with the original Norrbin model's accuracy of 78.12%. Adjusting the dimensionless cross-flow coefficients enabled the rapid identification of a curve that closely mirrored the sea trail. This research aimed to improve the accuracy of the Norrbin model and resolve issues related to determining the magnification of the hydrodynamic derivatives, laying a robust foundation for subsequent studies and applications in relevant domains.

Keywords: ship-turning circle; Norrbin model; dimensionless cross-flow coefficient; hydrodynamic derivatives



Citation: Li, G.; Chen, Y.; Yan, B.; Zhang, X. Refinement of Norrbin Model via Correlations between Dimensionless Cross-Flow Coefficient and Hydrodynamic Derivatives. *J. Mar. Sci. Eng.* **2024**, *12*, 752. <https://doi.org/10.3390/jmse12050752>

Academic Editors: Dong-Sheng Jeng and Rodolfo T. Gonçalves

Received: 29 February 2024

Revised: 27 April 2024

Accepted: 27 April 2024

Published: 30 April 2024



Copyright: © 2024 by the authors. Licensee MDPI, Basel, Switzerland. This article is an open access article distributed under the terms and conditions of the Creative Commons Attribution (CC BY) license (<https://creativecommons.org/licenses/by/4.0/>).

1. Introduction

Ship maneuverability, also referred to as ship motion performance, is a vital factor in maritime operations, serving as a key indicator that impacts ship design and the advancement of the international shipping industry. In 2002, the International Maritime Organization (IMO) embraced the Ship Maneuverability Standard Resolution MSC.137(76) [1], laying out essential criteria that ships are required to adhere to [2]. Without regard to the influence of the navigation environment, that is, the water and the depth of the water are not limited [3], the IMO Ship Maneuverability Standard evaluates a ship's maneuverability based on six key properties: inherent stability [4], direction keeping, redirection, bow-rocking suppression [5], gyration, and stopping [6]. Maneuverability is fundamental in assessing a ship's steering performance, impacting various scenarios, such as ship collision avoidance [7], pulling off the pier [8], inshore sailing [9], and ship turning. Yim [10] investigated the effectiveness of executing full-rudder turns to rotate the ship [11]. It is a performance index that measures the size of the minimum water area occupied by the ship's rotary motion [12] and the degree of rapid rotation [13]. Particularly important in nautical practice, a ship's turning ability has been examined by many investigators. Gao [14] proposed a more comprehensive evaluation method for ship maneuverability based on cluster analysis of the IMO maneuverability index. Li [15] achieved the accurate measurement of ship model coordinates through self-winding ship model experiments. Kim [16] examined the turning characteristics of a KCS (KRISO container ship) model

in regular waves through free model experiments, and proposed the concept of a safety index and investigated its relationship with waves. Chillcce [17] proposed a numerical method to simulate the wave maneuvering of a ship to calculate ship motion in calm water and waves. Suzuki [18] developed a numerical simulation approach to estimate the 6DOF (six degrees of freedom) motion of a ship maneuvering in a regular wave and conduct free model tests. Their obtained results indicate that the proposed methodology can rationally capture the test results. Ren [19] established an effective adaptive Nomoto model to deal with the ship path-tracking problem. Yasukawa [20] employed the proposed hydrodynamic coefficients for KVLCC2 to predict ship motion. Guo [21] developed a new design approach for ship-tracking control based on the Norrbinn model with enhanced system stability. Liu [22] considered both random noise and switching control in the Norrbinn model to discuss the steering control of a ship and solve the adaptive control problem. Zhou [23] effectively implemented the PID controller based on the Norrbinn model. For this purpose, a closed-loop gain-shaping algorithm was adopted to solve the long delay time problem of large ship movement. In summary, the common methods for predicting the turning circle of a ship are the free self-sailing model testing method [24], computer numerical simulation method [25], and semi-empirical estimation method. Along with the development of computer technology, more and more numerical simulation methods have been extensively implemented in ship-turning-ability forecasting. The commonly used methodologies are the MMG model [9,26], the Norrbinn model [27], and the Nomoto model. Herein, a modified Norrbinn model was employed to examine the problem at hand.

The simulation of ship maneuvering motion is based on an accurate mathematical model [28,29]. As ship design continues to evolve toward larger size, faster speeds, more specialized functions, and modernization, the accuracy of the Norrbinn model increasingly falls short, necessitating significant improvements. Li [30] improved the accuracy of the model by scaling the hydrodynamic derivatives of the Norrbinn model, resulting in a high degree of agreement with the experimental results of the ship-turning-circle prediction, Zhang [31] confirmed the effectiveness of Norrbinn's four-dimensional nonlinear mathematical model and second-order closed-loop gain-shaping algorithm for design control strategies. The main aim was to ensure the safe navigation of ships in waters with various sea conditions, solving the problem of the adaptive control of ship heading. A close survey of the conducted research on ship maneuvering performance by the aforementioned researchers was reviewed. Li [32] revealed that ship maneuverability experiments have mainly focused on ship heading control and ship maneuverability simulations, and the Norrbinn model has been commonly utilized to perform ship control simulation experiments. However, the major problem is that the types of ships involved in the pilot tests are small, most of the ships simulated in the tests are below 100,000 tons, and there are no simulation tests on the maneuvering performance of large ships. Subsequently, to investigate whether the Norrbinn model still has a high degree of conformity to the maneuvering performance of large ships, it was improved by incorporating data from large ships. In this regard, Yang [33] enlarged the hydrodynamic derivatives of the Norrbinn model and investigated to test the turning circle of a 300,000-ton ballast displacement ship. They improved the Norrbinn model based on matching some hydrodynamic derivatives with two nonlinear force moment empirical formulas identified by Norrbinn and obtained a turning circle closer to the actual ship's path with higher accuracy. The dimensionless cross-flow coefficient was of concern to scholars several times in the above articles, and it was briefly passed over and a value was considered for it. More specifically, what factors are associated with its value and how its variation affects the ship's turning circle have not been thoroughly discussed.

The contributions of this research can be chiefly summarized in the following three items:

- (1) A generalization formula connecting the dimensionless cross-flow coefficients with the four hydrodynamic derivatives was designed.
- (2) This formula possesses a certain universality and aids ships in promptly predicting the turning circle.

- (3) The research methodology presented in this article efficiently simplifies the Norrbin model while enhancing its accuracy.

The other sections of this paper are organized as follows. In Chapter 2, the Norrbin model used in this paper is introduced. Chapter 3 investigates the effects of the dimensionless cross-flow coefficient and hydrodynamic derivatives on the turning circle of ships. The results obtained suggest similarities, prompting a detailed examination of a potential relationship between the two variables. Subsequently, the accurate analysis results of the impact of individual adjusted hydrodynamic derivatives on a ship’s turning circle are given, establishing a correlation through an exchange of communication data between different vessels. In Chapter 4, validation of the generalizability of the formulated equation by applying it to another ship is shown, demonstrating that the average discrepancy fell within the anticipated range.

2. Mathematical Modeling

The ship motion model of the state-space type is the essential basis for ship controller design. To enhance the accuracy of the model, the nonlinear hydrodynamic term (F'_{NON}), wind term (F'_{WIND}), and wave force term (F'_{WAVE}) can be added to the right-hand side of the nonlinear mathematical model of ship movement [30]. Then, the dimensionless mathematical model associated with the nonlinear ship motion can be organized into the following forms:

$$I'_{(2)} \dot{X}_{(2)} = P'_{(2)} X_{(2)} + Q'_{(2)} U + F'_{NON} + F'_{WIND} + F'_{WAVE} \tag{1}$$

$$\begin{cases} X_{(2)} = [v \ r]^T, U = \delta \\ I'_{(2)} = \begin{bmatrix} m' - Y'_v & L(m' x'_C - Y'_r) \\ m' x'_C - N'_v & L(I'_{zz} - N'_r) \end{bmatrix} \\ P'_{(2)} = \begin{bmatrix} \frac{V}{L} Y'_v & V(Y'_r - m') \\ \frac{V}{L} N'_v & V(N'_r - m' x'_C) \end{bmatrix} \\ Q'_{(2)} = \begin{bmatrix} \frac{V^2}{L} Y'_\delta \\ \frac{V^2}{L} N'_\delta \end{bmatrix} \end{cases} \tag{2}$$

where the superscript prime symbol “'” stands for the non-dimensionalization, m' refers to the ratio of m to $\rho L^3/2$, x'_C denotes the ratio of x_C and L , I'_{zz} represents the ratio of I_{zz} and $\rho L^5/2$, V is the total speed, v denotes the transverse velocity, r is the turning rate, $X_{(2)}$ is the state vector, U is the control input, m denotes the mass, I_{zz} is the moment of inertia of the ship’s mass around the vertical axis passing through the center of gravity, L is the length between perpendiculars, x_c denotes the longitudinal center of gravity, and ρ is the water density.

Additionally, $I'_{(2)}$, $P'_{(2)}$, and $Q'_{(2)}$ are the inertial force matrix, viscous force matrix, and rudder force matrix, respectively. Moreover, the required factors in Equation (2) can

be obtained from the 10 linear hydrodynamic derivative regression formulas collated by Clark [34], as illustrated in Equation (3):

$$\left\{ \begin{array}{l} Y'_\delta = \frac{3.0A_\delta}{L^2} \\ Y'_v = -\left[1 + \frac{0.40C_bB}{T}\right] \cdot \pi(T/L)^2 - 0.30Y'_\delta \\ Y'_\dot{v} = -\left[1 + 0.16C_bB/T - 5.1(B/L)^2\right] \cdot \pi(T/L)^2 \\ Y'_r = -\left[-1/2 + 2.2B/L - 0.080B/T\right] \cdot \pi(T/L)^2 + 0.15Y'_\delta \\ Y'_\dot{r} = -\left[0.67B/L - 0.0033(B/T)^2\right] \cdot \pi(T/L)^2 \\ N'_\delta = -\left(\frac{1}{2}\right)Y'_\delta \\ N'_v = -\left[1/2 + 2.4T/L\right] \cdot \pi(T/L)^2 + 0.15Y'_\delta \\ N'_\dot{v} = -\left[1.1B/L - 0.041B/T\right] \cdot \pi(T/L)^2 \\ N'_r = -\left[1/4 + 0.039B/T - 0.56B/L\right] \cdot \pi(T/L)^2 - 0.075Y'_\delta \\ N'_\dot{r} = -\left[\frac{1}{12} + \frac{0.017C_bB}{T} - \frac{0.33B}{L}\right] \cdot \pi(T/L)^2 \end{array} \right. \quad (3)$$

where B , T , C_b , and A_δ are the width of the ship, the draft, block coefficient, and the rudder's area, respectively, and Y'_v , N'_v , Y'_r , and N'_r represent the hydrodynamic derivatives of the ship itself.

Norrbin presented a concise expression for the nonlinear fluid force in the study of the ship parameter identification problem, which is presented as follows:

$$F'_{NON} = \begin{bmatrix} Y'_{NON} \\ N'_{NON} \end{bmatrix} = \begin{bmatrix} C_r f_Y(v, r) \\ C_r f_N(v, r) \end{bmatrix} \quad (4)$$

The calculations of $f_Y(v, r)$ and $f_N(v, r)$ are given in Equations (5) and (6):

$$f_Y(v, r) = \begin{cases} T \cdot r|r| \left[-\frac{1}{12} - \frac{1}{L^2} \left(\frac{v}{r}\right)^2\right] & -\infty < -\frac{1}{L} \frac{v}{r} < -\frac{1}{2} \\ T \cdot r|r| \left[-\frac{1}{2} \frac{1}{L} \frac{v}{r} - \frac{2}{3} \frac{1}{L^3} \left(\frac{v}{r}\right)^3\right] & -\frac{1}{2} \leq -\frac{1}{L} \frac{v}{r} \leq \frac{1}{2} \\ T \cdot r|r| \left[\frac{1}{12} + \frac{1}{L^2} \left(\frac{v}{r}\right)^2\right] & \frac{1}{2} < -\frac{1}{L} \frac{v}{r} < \infty \end{cases} \quad (5)$$

$$f_N(v, r) = \begin{cases} T \cdot r|r| \left[-\frac{1}{6} \frac{1}{L} \left(\frac{v}{r}\right)\right] & -\infty < -\frac{1}{L} \frac{v}{r} < -\frac{1}{2} \\ T \cdot r|r| \left[-\frac{1}{32} - \frac{1}{4} \frac{1}{L^2} \left(\frac{v}{r}\right)^2 + \frac{1}{6} \frac{1}{L^4} \left(\frac{v}{r}\right)^4\right] & -\frac{1}{2} \leq -\frac{1}{L} \frac{v}{r} \leq \frac{1}{2} \\ T \cdot r|r| \left[\frac{1}{6} \frac{1}{L} \left(\frac{v}{r}\right)\right] & \frac{1}{2} < -\frac{1}{L} \frac{v}{r} < \infty \end{cases} \quad (6)$$

where C_r denotes the dimensionless cross-flow coefficient, whose value is usually taken in the range of 0.3 to 0.8. Since the sea trail is commonly disturbed by wind, current, and other effects, the wind-generated wave model used in [30] can be employed to deal with the disturbance of wind, current, and waves.

3. Results

3.1. Effect of the Dimensionless Cross-Flow Coefficient on the Ship's Turning Circle Performance

In the Norrbin model, the range of the dimensionless cross-flow coefficient is 0.3–0.8. To investigate the effect of this coefficient on the turning performance of the ship, the authors employed the ship “Yuan Kun Yang” for the simulations, where its ship parameters are provided in Table 1. In the actual turning test of the ship, the sea state had 2–3 levels, the wind had three levels, the actual wind direction was 175.5°, the tide in the test area exhibited back-and-forth flow, the maximum speed of the rising tide was 2.5 kn, the associated flow direction was S, the maximum speed of the falling tide was 1.5 kn, the corresponding flow

direction was N, and the initial heading was 190.2°. In the simulation, we chose various values of the dimensionless cross-flow coefficient in the range of 0.3–0.8 to observe its effect on the ship’s turning performance, and the experimental results of the simulation are presented in Figure 1 and Table 2.

Table 1. Particulars of “Yuan Kun Yang”.

| Name | Symbol | Unit | Yuan Kun Yang |
|--------------------------------|----------|----------------|---------------|
| Length | L_{pp} | m | 324.000 |
| Width | B | m | 60.000 |
| Design draft | d | m | 20.500 |
| Displacement | Δ | t | 310,297 |
| Square coefficient | C_b | / | 0.8215 |
| Design speed | v_0 | kn | 18.7 |
| Longitudinal center of gravity | X_c | m | 9.91 |
| Area of rudder | A_d | m ² | 139.217 |
| Molded depth | T_d | m | 30.0 |

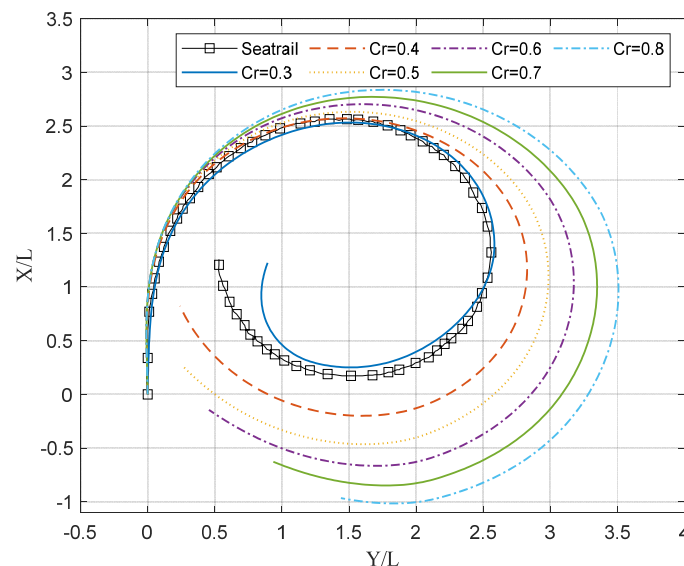


Figure 1. Diagram of the effect of the alerting dimensionless cross-flow coefficient C_r on ship turning.

Table 2. Parameter table of the influence of the dimensionless cross-flow coefficient on the turning circle.

| Category | $C_r = 0.3$ | $C_r = 0.4$ | $C_r = 0.5$ | $C_r = 0.6$ | $C_r = 0.7$ | $C_r = 0.8$ |
|---------------------------|-------------|-------------|-------------|-------------|-------------|-------------|
| A_{dmax}/L | 2.62 | 2.65 | 2.69 | 2.73 | 2.78 | 2.82 |
| A_{dmin}/L | 0.37 | 0.10 | −0.2 | −0.5 | −0.7 | −1.0 |
| T_{rmax}/L | 2.53 | 2.74 | 2.93 | 3.15 | 3.33 | 3.53 |
| $(A_{dmax} - A_{dmin})/L$ | 2.25 | 2.55 | 2.87 | 3.19 | 3.52 | 3.83 |

Figure 1 and Table 2 show the significant effect of the variation of the dimensionless cross-flow coefficient on the turning circle of the ship. The simulation results indicate that the turning circle of the ship grew with the growth of the dimensionless cross-flow coefficient, and generally, the longitudinal growth was substantially lower than the transverse growth.

3.2. Influence of the Hydrodynamic Conductivity on the Rotational Performance

To investigate the effect of the hydrodynamic derivatives on the ship’s turning circle performance, “Yuan Kun Yang” was again utilized for the simulations. To explore the effect

of the magnification of hydrodynamic derivatives, its value was considered in the range of 1.1 to 1.6. The hydrodynamic derivatives on the turning circle of the ship and the obtained simulation results are presented in Figure 2 and Table 3.

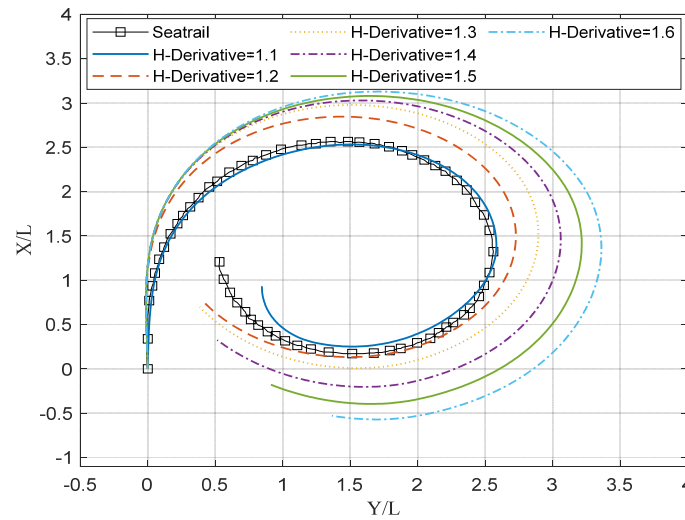


Figure 2. Effects of the various hydrodynamic derivatives on the ship’s turning circle.

Table 3. Parameter table of influence of the hydrodynamic derivative magnification on the ship’s turning circle.

| Category | 1.1 Times | 1.2 Times | 1.3 Times | 1.4 Times | 1.5 Times | 1.6 Times |
|---------------------------|-----------|-----------|-----------|-----------|-----------|-----------|
| A_{dmax}/L | 2.61 | 2.72 | 2.83 | 2.94 | 3.05 | 3.17 |
| A_{dmin}/L | 0.39 | 0.30 | 0.16 | 0.00 | −0.2 | −0.5 |
| T_{rmax}/L | 2.57 | 2.73 | 2.92 | 3.13 | 3.35 | 3.60 |
| $(A_{dmax} - A_{dmin})/L$ | 2.22 | 2.42 | 2.67 | 2.94 | 3.26 | 3.64 |

From Figure 2 and Table 3, it is clear that changing the hydrodynamic derivatives had the same significant effect on the turning circle of the ship. The simulation results show that the turning circle of the ship increased with the growth of the hydrodynamic derivatives, and the longitudinal growth was slightly smaller than the transverse growth.

By comparing Tables 2 and 3, it was found that both the enlargement of the dimensionless cross-flow coefficient and the enlargement of the hydrodynamic derivative could combine to significantly increase the turning circle of the ship. In addition, the increasing effect of the hydrodynamic derivative in the longitudinal distance of the turning circle was greater than the dimensionless cross-flow coefficient, and the discrepancies between these two were not significant in increasing the transverse distance of the ship’s turning circle.

3.3. Influence of the Single Amplified Hydrodynamic Conductivity on the Ship’s Turning Circle Performance

Based on navigational practices, it was discovered that after the enlargement of ships, the forces and moments related to the yaw rate and yaw acceleration increased. To examine the effect of a single magnification of hydrodynamic derivatives on the ship-turning circle, the magnification was chosen to select various values in the range of 1.1–1.6, while the magnification values of other hydrodynamic derivatives were kept fixed. The obtained results reveal that when the hydrodynamic derivatives were all amplified by 1.1 times, the formed turning circle was the most consistent with the actual ship trajectory. Therefore, we set the hydrodynamic derivatives to be enlarged by 1.1 times, adjusted the value of a specific hydrodynamic derivative to ensure that there was only one variable in the simulation, and adopted the “Yuan Kun Yang” simulation. For the sake of convenience in plotting

the results, the simulation results are illustrated in Figure 3, which are represented in the graph respectively.

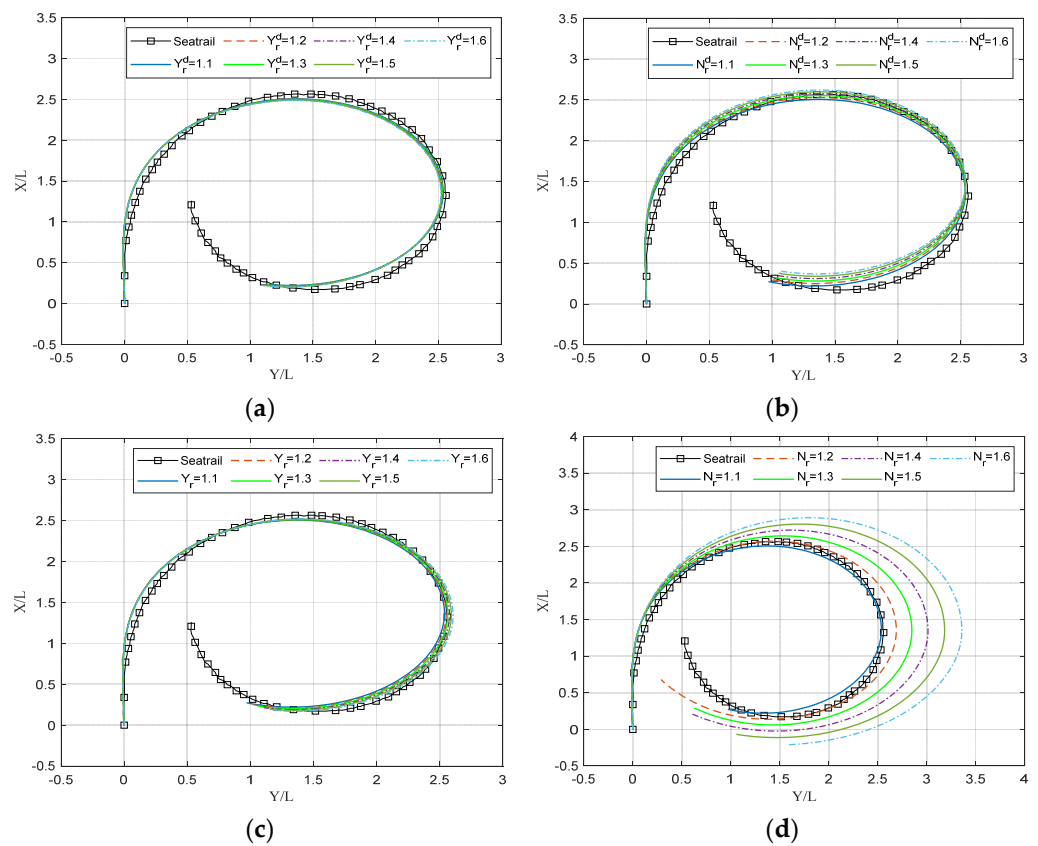


Figure 3. Diagram of the effects of single magnification of Y_r^l , N_r^l , Y_r^d , and N_r^d on ship-turning performance. (a) Comparison with only Y_r^l changing. (b) Comparison with only N_r^l changing. (c) Comparison with only Y_r^d changing. (d) Comparison with only N_r^d changing.

According to Figure 3, it can be seen that the effect of the single amplification on the turning circle changed after different degrees of single amplification of the hydrodynamic derivative, and the influence law of single amplification on the turning circle was also presented in Table 4.

Table 4. Table of the effect of single magnification of Y_r^l , N_r^l , Y_r^d , and N_r^d on ship-turning circle.

| Category | Max. Longitudinal Front Distance | Max. Longitudinal Aft Distance | Maximum Horizontal Distance | Integral Turning Circle |
|-------------------------|----------------------------------|--------------------------------|-----------------------------|-------------------------|
| Single enlarged Y_r^l | Slightly smaller | Slightly larger | Slightly smaller | Slightly down |
| Single enlarged N_r^l | Larger | Smaller | Virtually unchanged | Upward |
| Single enlarged Y_r^d | Slightly larger | Larger | Larger | Downward |
| Single enlarged N_r^d | Significantly larger | Significantly larger | Significantly larger | Significantly larger |

From Table 4, it can be seen that after the increase in the single magnification, the first longitudinal distance of the ship circle was slightly reduced and the trailing longitudinal distance was slightly increased. Furthermore, the change in the transverse distance was not clear, and the overall circle was slightly shifted downward. After the single magnification, the first longitudinal distance of the ship circle grew, the trailing longitudinal distance lessened, the transverse distance almost remained unchanged, and the overall circle was shifted upward. After the single magnification, the first longitudinal distance of the ship circle was slightly increased, the trailing longitudinal distance grew, the transverse

distance also enlarged, and the overall circle was shifted downward. Finally, after the single magnification, the first longitudinal distance of the ship circle substantially grew, the trailing longitudinal distance noticeably grew, the transverse distance also increased significantly, and the overall circle increased significantly.

The main conclusions obtained from Table 4 and Figure 3 can be summarized as follows: Y'_r had a minimal effect on the turning circle, N'_r had a greater effect on the longitudinal distance, Y'_r had a greater effect on the transverse distance, and N'_r was the main influential factor of the turning circle.

3.4. Investigation of the Relationship between the Dimensionless Cross-Flow Coefficient and the Hydrodynamic Derivatives

In conclusion, the change in the dimensionless cross-flow coefficient and the hydrodynamic derivatives both had remarkable and similar impacts on the turning circle of the ship, and thereby, the effect of a single change on the turning circle of the ship was methodically planned. In theory, by unequally scaling the hydrodynamic derivatives, a turning circle could be obtained that was approximately equivalent to the variation in the dimensionless cross-flow coefficient. To investigate the relationship between the dimensionless cross-flow coefficient and the hydrodynamic derivative, the following simulation was performed: after first matching with C_r (i.e., in the cases of 1.6 and 0.8, the turning circles were similar; therefore, in the case of 0.8, N'_r was 1.6, and the others could be sequentially matched), N'_r was reduced to adjust the longitudinal distance, Y'_r was altered to adjust the transverse distance, and finally Y'_r was changed to achieve a fine adjustment of the turning circle.

The simulation results are presented In Table 5 and Figure 4, and the curve-fitting results were found, as illustrated in Figure 5. These are collated in Equation (7):

$$\begin{cases} fdY'_r = 16.9C_r - 5.37 \\ fdN'_r = -1.5C_r + 1.41 \\ fdY'_r = 1.782 \sin(2.454C_r + 6.208) \\ fdN'_r = C_r + 0.8 \end{cases} \quad (7)$$

where C_r represents the dimensionless cross-flow coefficient, whose value in the simulation was taken in the range of 0.4 to 0.7. The factors fdN'_r , fdN'_r , fdY'_r , and fdN'_r denote the magnifications of Y'_r , N'_r , Y'_r , and N'_r , respectively. It is noteworthy that the corresponding four formulations could be adopted to fit the dimensionless cross-flow coefficient changes by the curve fitting toolbox in MATLAB, and unequal scaling of Y'_r , N'_r , Y'_r , and N'_r was utilized to form the turning circle. Hence, the four magnification values must be determined based on the value of one given C_r and only one so that the resulting correspondences will be meaningful.

Table 5. Table of the corresponding relation between unequal scaling of the hydrodynamic derivatives and the dimensionless cross-flow coefficient.

| C_r | N'_r | N'_r | Y'_r | Y'_r |
|-------|--------|--------|--------|--------|
| 0.4 | 1.2 | 0.80 | 1.400 | 1.5 |
| 0.5 | 1.3 | 0.68 | 1.635 | 3.0 |
| 0.6 | 1.4 | 0.50 | 1.748 | 4.6 |
| 0.7 | 1.5 | 0.36 | 1.780 | 6.6 |

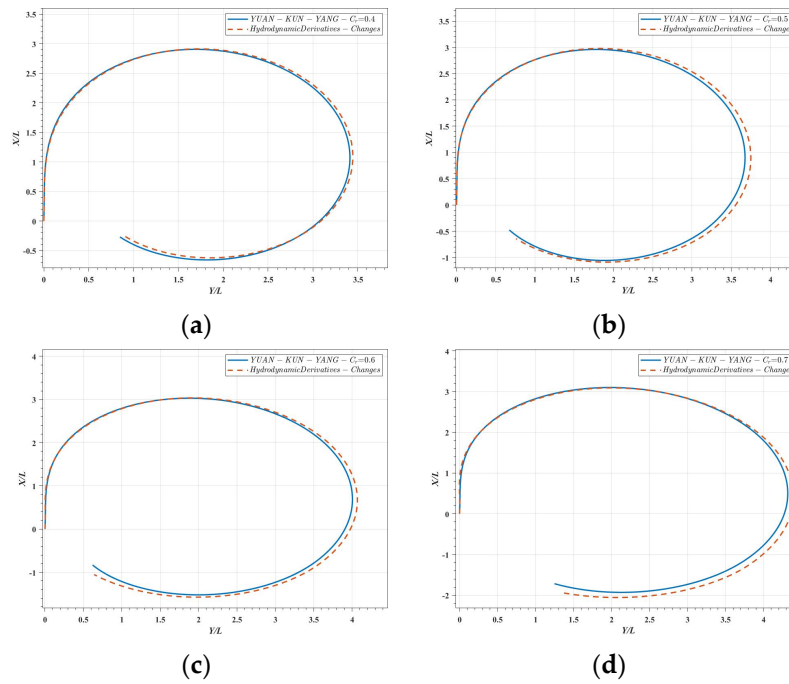


Figure 4. Contrast diagram of turning circle with various dimensionless cross-flow coefficients by unequal scaling of the hydrodynamic derivatives. (a) Comparison with changing derivatives and $C_r = 0.4$. (b) Comparison with changing derivatives and $C_r = 0.5$. (c) Comparison with changing derivatives and $C_r = 0.6$. (d) Comparison with changing derivatives and $C_r = 0.7$.

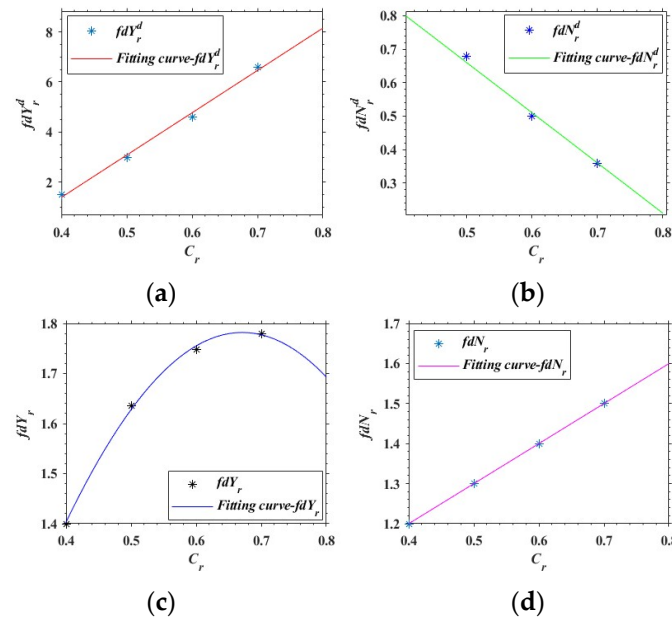


Figure 5. Fitting curve. (a) Fitting for Y'_r . (b) Fitting for N'_r . (c) Fitting for Y'_r . (d) Fitting for N'_r .

To check whether Equation (7) is still applicable for other ships, seven other different ships with tonnages ranging from 50,000 tons to 300,000 tons and different types of bulk carriers, container ships, and tankers were selected, where the data of the ship type parameters are presented in Table 6.

Table 6. Ship type data parameters.

| Name | Symbol | Unit | Monte Granada | Pacific Sapphire | Yuan Kun Yang | KVLCC2 | Hanover Square | Emerald Splendor | Long Hu San | Saturn Moon |
|-------------------|----------|------|---------------|------------------|---------------|------------|----------------|------------------|-------------|-------------|
| Ship type | / | / | Bulk carrier | Oil tanker | Oil tanker | Oil tanker | Bulk carrier | Container vessel | Oil tanker | Oil tanker |
| Length | L_{pp} | m | 274.20 | 179.99 | 324.00 | 320.00 | 249.90 | 228.00 | 333.00 | 274.00 |
| Width | B | m | 48.00 | 32.20 | 60.00 | 58.00 | 44.00 | 32.24 | 60.00 | 48.00 |
| Draft | d | m | 15.30 | 12.62 | 20.50 | 20.80 | 21.50 | 12.22 | 21.00 | 17.15 |
| Displacement | Δ | t | 173,054 | 58,025 | 310,290 | 312,600 | 64,200 | 74,789 | 366,534 | 168,729 |
| Block coefficient | C_b | / | 0.781 | 0.8095 | 0.8215 | 0.81 | 0.8085 | 0.8430 | 0.821 | 0.8026 |
| Speed | v_0 | kn | 15.73 | 15.30 | 18.7 | 15.8 | 14.45 | 15.60 | 12.20 | 13.1 |
| Molded depth | T_d | m | 22.40 | 19.05 | 30.00 | 30.00 | 30.00 | 20.65 | 30.50 | 23.40 |

Then, using the simulation of other ship data according to the above steps, the matching between Y'_r, N'_r, Y'_r, N'_r , and C_r is organized in Table 7, which was found by fitting the respective formulas. Finally, a set of formulas for the dimensionless cross-flow coefficients was obtained by averaging the coefficients in each formula, as provided in the following:

$$\begin{cases} fdY'_r = 17.781C_r - 6.044 \\ fdN'_r = -1.182C_r + 1.286 \\ fdY'_r = 1.877 \sin(0.971C_r + 7.040) \\ fdN'_r = 0.992C_r + 0.779 \end{cases} \quad (8)$$

Table 7. Ship's C_r and Y'_r, N'_r, Y'_r , and N'_r correspondence.

| Yuan Kun Yang | | | | | Monte Granada | | | | |
|------------------|--------|--------|--------|--------|---------------|--------|--------|--------|--------|
| C_r | N'_r | N'_r | Y'_r | Y'_r | C_r | N'_r | N'_r | Y'_r | Y'_r |
| 0.4 | 1.2 | 0.80 | 1.400 | 1.5 | 0.4 | 1.2 | 0.78 | 1.4 | 1.39 |
| 0.5 | 1.3 | 0.68 | 1.635 | 3.0 | 0.5 | 1.3 | 0.6 | 1.3 | 3.08 |
| 0.6 | 1.4 | 0.50 | 1.748 | 4.6 | 0.6 | 1.42 | 0.5 | 1.25 | 6.4 |
| 0.7 | 1.5 | 0.36 | 1.780 | 6.6 | 0.7 | 1.55 | 0.36 | 1.1 | 8.0 |
| Hanover Square | | | | | KVLCC2 | | | | |
| C_r | N'_r | N'_r | Y'_r | Y'_r | C_r | N'_r | N'_r | Y'_r | Y'_r |
| 0.4 | 1.2 | 0.81 | 1.403 | 1.39 | 0.4 | 1.15 | 0.81 | 1.403 | 1.39 |
| 0.5 | 1.3 | 0.66 | 1.298 | 3.08 | 0.5 | 1.21 | 0.66 | 1.628 | 3.08 |
| 0.6 | 1.4 | 0.51 | 1.2 | 4.77 | 0.6 | 1.29 | 0.51 | 1.755 | 4.77 |
| 0.7 | 1.5 | 0.36 | 1.1 | 6.46 | 0.7 | 1.37 | 0.36 | 1.777 | 6.46 |
| Pacific Sapphire | | | | | Long Hu San | | | | |
| C_r | N'_r | N'_r | Y'_r | Y'_r | C_r | N'_r | N'_r | Y'_r | Y'_r |
| 0.4 | 1.2 | 0.78 | 1.4 | 1.39 | 0.4 | 1.2 | 0.7 | 1.3 | 1.5 |
| 0.5 | 1.3 | 0.6 | 1.3 | 3.08 | 0.5 | 1.3 | 0.6 | 1.25 | 2.5 |
| 0.6 | 1.4 | 0.5 | 1.0 | 4.0 | 0.6 | 1.4 | 0.5 | 1.22 | 5.0 |
| 0.7 | 1.5 | 0.4 | 0.9 | 5.2 | 0.7 | 1.5 | 0.4 | 1.18 | 6.4 |
| Emerald Splendor | | | | | Saturn Moon | | | | |
| C_r | N'_r | N'_r | Y'_r | Y'_r | C_r | N'_r | N'_r | Y'_r | Y'_r |
| 0.4 | 1.2 | 0.8 | 1.20 | 1.5 | 0.4 | 1.2 | 0.8 | 1.20 | 1.5 |
| 0.5 | 1.3 | 0.7 | 1.15 | 3.5 | 0.5 | 1.3 | 0.7 | 1.15 | 3.0 |
| 0.6 | 1.4 | 0.6 | 1.10 | 6.0 | 0.6 | 1.4 | 0.6 | 1.10 | 5.5 |
| 0.7 | 1.5 | 0.5 | 1.05 | 9.0 | 0.7 | 1.5 | 0.55 | 1.05 | 7.0 |

The hydrodynamic derivatives for various values (i.e., 0.4, 0.5, 0.6, and 0.7) were then appropriately evaluated using Equation (8), and the corresponding values are summarized in Table 8.

Table 8. The corresponding relationships between C_r and Y'_r , N'_r , Y'_r , and N'_r in Formula (9).

| C_r | fdY'_r | fdN'_r | fdY'_r | fdN'_r |
|-------|----------|----------|----------|----------|
| 0.4 | 1.069 | 0.813 | 1.709 | 1.176 |
| 0.5 | 2.847 | 0.695 | 1.776 | 1.275 |
| 0.6 | 4.625 | 0.576 | 1.827 | 1.375 |
| 0.7 | 6.403 | 0.458 | 1.860 | 1.474 |

4. Simulation Tests

Let us introduce a ship called “Cesi Gladstone” to validate Equation (8), where the parameters of the ship are given in Table 9. In addition, the sea state of the sea area was assumed to have 1–2 levels, and the wind force was considered at four levels, and the wind direction was 47.6° . The tides in the offshore area had an alternating current, the maximum speed of the high tide was 1.5 kn, the flow direction was SW, the maximum speed of the falling tide was 1.0 kn, the current direction was NE, and the initial heading was set to 107° . The dimensionless cross-flow coefficients were considered as 0.4, 0.5, 0.6, and 0.7, the corresponding hydrodynamic derivatives are presented in Table 8, and the simulation results are demonstrated in Figure 6.

Table 9. “Cesi Gladstone” main parameters.

| Name | Symbol | Unit | Cesi Gladstone |
|-------------------|----------|------|----------------|
| Length | L_{pp} | m | 290.000 |
| Width | B | m | 45.600 |
| Design draft | d | m | 11.70 |
| Displacement | Δ | t | 120,686.5 |
| Block coefficient | C_b | / | 0.8022 |
| Design speed | v_0 | kn | 14.0 |
| Molded depth | T_d | m | 26.50 |

To quantify the research results, this study referred to the compliance algorithm in [29] and selected the maximum longitudinal distance in the forward direction, the maximum longitudinal distance in the backward direction, and the maximum distance in the transverse direction. The direction and the maximum distance difference in the longitudinal direction were used as evaluation indices of the ship’s turning performance. Then, the average compliance of the ship’s turning performance was appropriately calculated, which is presented in Equation (9). In this relation, A_{dmax} denotes the maximum longitudinal distance in the first direction, A_{dmin} represents the maximum longitudinal distance in the first direction, T_{rmax} stands for the maximum longitudinal distance in the transverse direction, $A_{dmax-dmin}$ signifies the maximum longitudinal distance difference, and \bar{C}_M denotes the average compliance.

$$\bar{C}_M = \frac{1}{4} \left(\frac{\min(A_{dmax_true}, A_{dmax_model})}{\max(A_{dmax_true}, A_{dmax_model})} + \frac{\min(A_{dmin_true}, A_{dmin_model})}{\max(A_{dmin_true}, A_{dmin_model})} + \frac{\min(T_{rmax_true}, T_{rmax_model})}{\max(T_{rmax_true}, T_{rmax_model})} + \frac{\min(A_{dmax_true-dmin_true}, A_{dmax_model-dmin_model})}{\max(A_{dmax_true-dmin_true}, A_{dmax_model-dmin_model})} \right) \times 100\% \tag{9}$$

Given the space limitation, only some compliance calculations are given, and note the distinction in Table 10, where \bar{C}_{M1} represents the calculated compliance of C_r and its derivatives show the turning circle with the real ship trajectory, and \bar{C}_{M2} indicates the calculated compliance of C_r with changing hydrodynamic derivatives to form two turning circles. Subsequently, the average compliance difference between C_r and the corresponding hydrodynamic derivatives that formed the turning circle and the real ship trail was calculated, as the results are provided in Table 11.

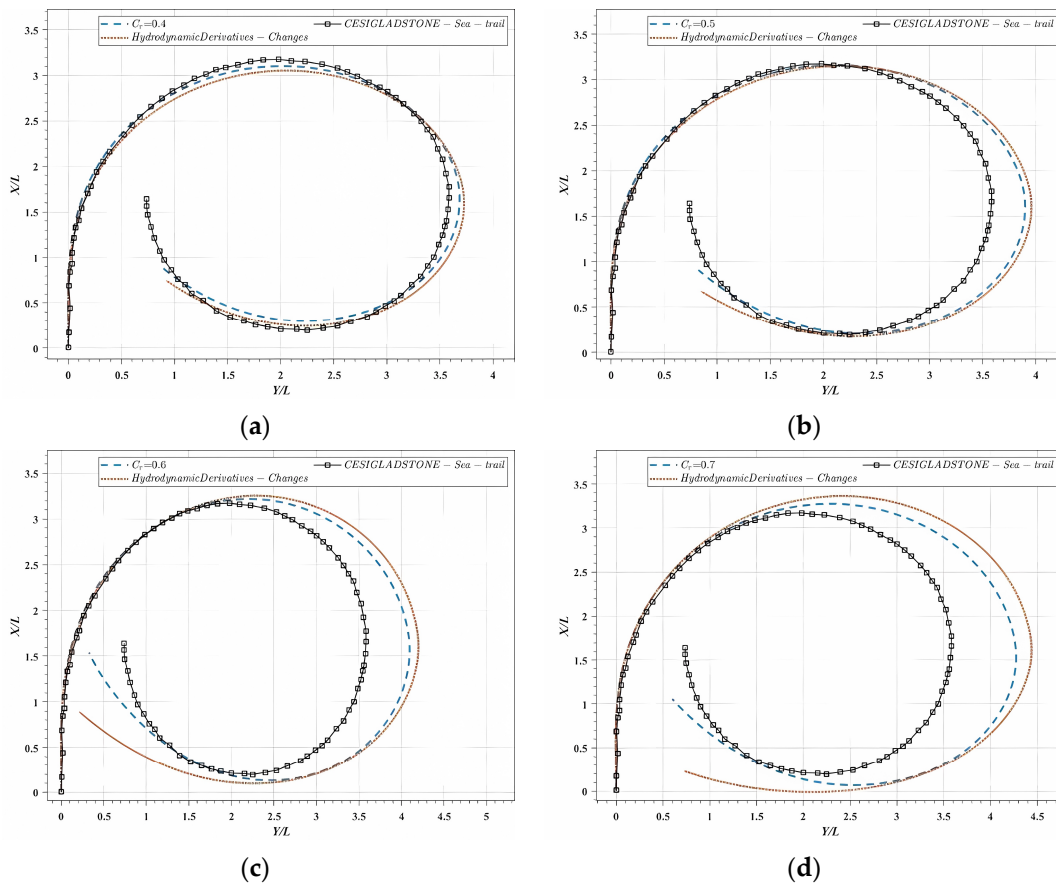


Figure 6. Diagram of the influence of the dimensionless cross-flow coefficient and the hydrodynamic derivatives on the “Cesi Gladstone” turning performance. (a) Comparison with changing sea trail, derivatives, and $C_r = 0.4$. (b) Comparison with changing sea trail, derivatives, and $C_r = 0.5$. (c) Comparison with changing sea trail, derivatives, and $C_r = 0.6$. (d) Comparison with changing sea trail, derivatives, and $C_r = 0.7$.

Table 10. “Cesi Gladstone” wheel ship-turning test parameter table.

| Category | $C_r = 0.4$ | Derivatives | $C_r = 0.5$ | Derivatives | Sea Trajectory |
|---------------------------|-------------|-------------|-------------|-------------|----------------|
| A_{dmax}/L | 3.10 | 3.05 | 3.12 | 3.11 | 3.17 |
| A_{dmin}/L | 0.31 | 0.25 | 0.18 | 0.21 | 0.20 |
| T_{rmax}/L | 3.68 | 3.72 | 3.89 | 3.96 | 3.58 |
| $(A_{dmax} - A_{dmin})/L$ | 2.89 | 2.80 | 2.98 | 2.93 | 2.97 |
| \bar{C}_{M1} | 89.22% | 91.68% | 85.19% | 87.23% | / |
| \bar{C}_{M2} | 93.10% | | 92.37% | | / |

Table 11. “Cesi Gladstone” round coincidence difference table.

| C_r | $C_r = 0.4$ | $C_r = 0.5$ | $C_r = 0.6$ | $C_r = 0.7$ | Average |
|-------------------------|-------------|-------------|-------------|-------------|---------|
| Conformity difference | 2.24% | 2.47% | 2.91% | 3.18% | 2.70% |
| Contrast correspondence | 93.10% | 92.37% | 91.91% | 91.39% | 92.19% |

Table 11 presents the average difference between the turning circle formed by the dimensionless cross-flow coefficient and its corresponding changing hydrodynamic derivative. The conformity difference is the difference in \bar{C}_{M1} between different dimensionless cross-flow coefficients and their corresponding hydrodynamic derivatives. The contrast

correspondence is the average compliance rate between different dimensionless cross-flow coefficients and their corresponding hydrodynamic derivatives. The obtained results reveal that the conformity difference for the turning circle of the real ship trajectory was predicted to be 2.70% and the average contrast between the two circles was obtained as 92.19%, which fulfilled the expected purpose and showed that Equation (8) had a certain generalization to different ships. The next step was to check whether the accuracy of the simplified model was improved. To this end, the simulation of the “Cesi Gladstone” ship was combined with the Norrbín model and the turning circle, which was formed by changing the dimensionless cross-flow coefficient and the corresponding hydrodynamic derivatives, and the calculated results are presented in Figure 7 and Table 12.

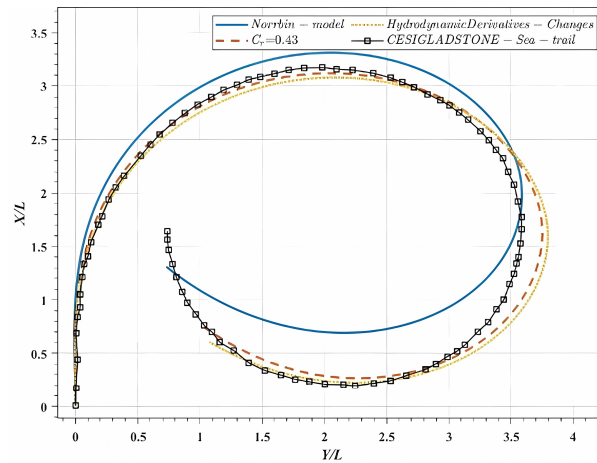


Figure 7. “Cesi Gladstone” ship formula verification diagram.

Table 12. Table of turning test parameters of the ship “Cesi Gladstone”.

| Category | Norrbín Model | $C_r = 0.43$ | Derivative | Sea Trajectory |
|---------------------------|---------------|--------------|------------|----------------|
| A_{dmax}/L | 3.17 | 3.10 | 3.08 | 3.17 |
| A_{dmin}/L | 0.69 | 0.26 | 0.23 | 0.20 |
| T_{rmax}/L | 3.58 | 3.75 | 3.79 | 3.58 |
| $(A_{dmax} - A_{dmin})/L$ | 2.48 | 2.84 | 2.85 | 2.97 |
| \bar{C}_M | 78.12% | 91.45% | 92.87% | / |

The simulation results reveal that the correspondence of the turning circle with the real ship trajectory obtained using the original Norrbín model was obtained as 78.12%, while after adjusting C_r and related hydrodynamic derivatives, the correspondence of the final turning circles with the real ship trajectory were obtained as 91.45% and 92.87%. These values are remarkably higher than that predicted by the original Norrbín model, and the correspondence of the two was very close to the real ship trajectory. The simulation results indicate that the accuracy of the simplified model was also improved.

5. Conclusions

In this study, the impact of the dimensionless cross-flow coefficient and the variations in four hydrodynamic derivative factors on the ship’s turning circle were systematically analyzed. Correlation equations linking the dimensionless cross-flow coefficient to the four hydrodynamic derivative factors were successfully developed. Simulation results demonstrated that our formulated model achieved an average consistency of 90.24% across diverse vessel types. Through adjustments to the dimensionless cross-flow coefficient, a highly accurate representation of the actual ship trajectory could be rapidly achieved. By considering the interplay between the dimensionless cross-flow coefficient and the four hydrodynamic derivative factors, and the individual influence of each hydrodynamic

derivative on the ship's turning circle, the four factors were proportionally scaled and appropriately adjusted to swiftly and effectively enhance the accuracy in aligning with the real ship trajectory. This approach is crucial for refining the prediction accuracy of the ship's turning circle post changes in wind flow, thereby ensuring navigational safety. However, there is room for further refinement in current research, particularly in examining slight variations in the square coefficients and the effects of increased speed. Given the limited availability of ship data, future studies will focus on expanding data collection efforts to refine Equation (8), bolster the accuracy of the Norrbin model, optimize prediction outcomes, and ultimately fortify navigational security.

Author Contributions: Conceptualization, G.L. and X.Z.; methodology, X.Z.; software, G.L.; validation, G.L., B.Y. and Y.C.; formal analysis, Y.C.; investigation, Y.C.; resources, B.Y.; data curation, Y.C.; writing—original draft preparation, B.Y. and Y.C.; writing—review and editing, Y.C. and G.L.; visualization, G.L.; supervision, X.Z.; project administration, X.Z.; funding acquisition, G.L. All authors have read and agreed to the published version of the manuscript.

Funding: This work was partially supported by the National Natural Science Foundation of China (grant no. 51679024), Dalian Innovation Team Support Plan in the Key Research Field (2020RT08), the Fundamental Research Funds for the Central Universities (3132023502), and the 2023 DMU Navigation College first-class interdisciplinary research project (2023JXA06).

Institutional Review Board Statement: Not applicable.

Informed Consent Statement: Not applicable.

Data Availability Statement: The data presented in this study are available on request from the corresponding author. The data are not publicly available due to privacy.

Acknowledgments: The authors would like to thank anonymous reviewers for their valuable comments to enhance the quality of this article.

Conflicts of Interest: The authors declare no conflicts of interest.

References

1. Landsburg, A.C.; Barr, R.A.; Daggett, L.; Hwang, W.Y.; Jakobsen, B.; Morris, M.; Vest, L. Critical needs for ship maneuverability: Lessons from the Houston ship channel full-scale maneuvering trials. *Mar. Technol. SNAME N.* **2005**, *42*, 11–20. [[CrossRef](#)]
2. Wang, X.; Liu, Z.J.; Cai, Y. A Rating Based Fuzzy Analytic Network Process (F-ANP) Model for Evaluation of Ship Maneuverability. *Ocean Eng.* **2015**, *106*, 39–46. [[CrossRef](#)]
3. Yuan, Y.P.; Li, Z.X.; Malekian, R.; Yan, X.P. Analysis of the Operational Ship Energy Efficiency Considering Navigation Environmental Impacts. *J. Mar. Eng. Technol.* **2017**, *16*, 150–159. [[CrossRef](#)]
4. Woo, D.; Choe, H.; Im, N. Analysis of the Relationship Between GM and IMO Intact Stability Parameters to Propose Simple Evaluation Methodology. *J. Mar. Sci. Eng.* **2021**, *9*, 735. [[CrossRef](#)]
5. Ding, S.X.; Zhao, T.S.; Gao, F.; Tang, Z.F.; Jin, B.Q. Research on a Motion-Inhibition Fuzzy Control Method for Moored Ship with Multi-Robot System. *Ocean Eng.* **2022**, *248*, 110795. [[CrossRef](#)]
6. Yin, J.C.; Perakis, A.N.; Wang, N. A Real-Time Ship Roll Motion Prediction Using Wavelet Transform and Variable RBF Network. *Ocean Eng.* **2018**, *160*, 10–19. [[CrossRef](#)]
7. Zhang, G.Y.; Wang, Y.; Liu, J.; Cai, W.; Wang, H.B. Collision-Avoidance Decision System for Inland Ships Based on Velocity Obstacle Algorithms. *J. Mar. Sci. Eng.* **2022**, *10*, 814. [[CrossRef](#)]
8. Wu, L.H.; Li, Y.P.; Su, S.J.; Yan, P.; Qin, Y. Hydrodynamic Analysis of AUV Underwater Docking with a Cone-Shaped Dock Under Ocean Currents. *Ocean Eng.* **2014**, *85*, 110–126. [[CrossRef](#)]
9. Li, S.L.; Liu, C.G.; Chu, X.M.; Zheng, M.; Wang, Z.P.; Kan, J.Y. Ship Maneuverability Modeling and Numerical Prediction Using CFD with Body Force Propeller. *Ocean Eng.* **2022**, *264*, 112454. [[CrossRef](#)]
10. Yim, J.B.; Park, D.J. Estimating Critical Latency Affecting Ship's Collision in Re-Mote Maneuvering of Autonomous Ships. *Appl. Sci.* **2021**, *11*, 10987. [[CrossRef](#)]
11. Hua, L.L.; Peng, Z.; Tao, Z.S.; Ming, J.; Jia, Y. Simulation Analysis of Fin Stabilizer on Ship Roll Control During Turning Motion. *Ocean Eng.* **2018**, *164*, 733–748.
12. Kang, L.J.; Meng, Q.; Zhou, C.B.; Gao, S. How Do Ships Pass through L-Shaped Turnings in the Singapore Strait? *Ocean Eng.* **2019**, *182*, 329–342. [[CrossRef](#)]
13. Song, M.H.; Pham, X.D.; Vuong, Q.D. Torsional Vibration Stress and Fatigue Strength Analysis of Marine Propulsion Shafting System Based on Engine Operation Patterns. *J. Mar. Sci. Eng.* **2020**, *8*, 613. [[CrossRef](#)]

14. Gao, H.; Zou, Z.; Xia, L.; Yuan, S. Application of the NIPC-Based Uncertainty Quantification in Prediction of Ship Maneuverability. *J. Mar. Eng. Technol.* **2021**, *26*, 555–572. [[CrossRef](#)]
15. Li, Z.H.; Zhou, Y.G.Z.; Wu, J.; Shu, Y.J.; Han, P. Route Tracking for Self-Propelled Ship Model. *Multimed. Tools. Appl.* **2019**, *78*, 4365–4379. [[CrossRef](#)]
16. Kim, D.J.; Yun, K.H.; Yeo, D.J.; Kim, Y.G. Initial and Steady Turning Characteristics of KCS in Regular Waves. *Appl. Ocean Res.* **2020**, *105*, 102421. [[CrossRef](#)]
17. Chillcce, G.; el Moctar, O. A Numerical Method for Manoeuvring Simulation in Regular Waves. *Ocean Eng.* **2018**, *170*, 434–444. [[CrossRef](#)]
18. Suzuki, R.; Ueno, M.; Tsukada, Y. Numerical Simulation of 6-Degrees-of-Freedom Motions for a Manoeuvring Ship in Regular Waves. *Appl. Ocean Res.* **2021**, *113*, 102732. [[CrossRef](#)]
19. Ren, R.Y.; Zou, Z.J.; Wang, Y.D.; Wang, X.G. Adaptive Nomoto Model Used in the Path Following Problem of Ships. *J. Mar. Sci. Technol.* **2018**, *23*, 888–898. [[CrossRef](#)]
20. Yasukawa, H.; Yoshimura, Y. Introduction of MMG Standard Method for Ship Maneuvering Predictions. *J. Mar. Sci. Technol.* **2015**, *20*, 37–52. [[CrossRef](#)]
21. Guo, M.C.; Xu, D.B.; Liu, L. Adaptive Nonlinear Ship Tracking Control with Unknown Control Direction. *Int. J. Robust Nonlinear Control.* **2018**, *28*, 2828–2840. [[CrossRef](#)]
22. Liu, Y.L.; Wang, R.Z.; Zhao, Y.C.; Mu, D.D. Td-Based Adaptive Output Feedback Control of Ship Heading with Stochastic Noise and Unknown Actuator Dead-Zone Input. *Appl. Sci.* **2022**, *12*, 1985. [[CrossRef](#)]
23. Zhou, Z.G.; Zhang, Y.J.; Wang, S.B. A Coordination System Between Decision Making and Controlling for Autonomous Collision Avoidance of Large Intelligent Ships. *J. Mar. Sci. Eng.* **2021**, *9*, 1202. [[CrossRef](#)]
24. Serani, A.; Dragone, P.L.; Stern, F.; Diez, M. On the Use of Dynamic Mode Decomposition for Time-Series Forecasting of Ships Operating in Waves. *Ocean Eng.* **2023**, *267*, 113235. [[CrossRef](#)]
25. Van Der Kolk, N.J.; Akkerman, I.; Keuning, J.A.; Huijsmans, R.H.M. Part 2: Simulation Methodology and Numerical Uncertainty for Rans-CFD for the Hydrodynamics of Wind-Assisted Ships Operating at Leeway Angles. *Ocean Eng.* **2020**, *201*, 107024. [[CrossRef](#)]
26. Yasukawa, H.; Ishikawa, T.; Yoshimura, Y. Investigation on the Rudder Force of a Ship in Large Drifting Conditions with the MMG Model. *J. Mar. Sci. Technol.* **2021**, *26*, 1078–1095. [[CrossRef](#)]
27. Norrbin, N.H.; Bystrom, L.; Astrom, K.J. *Further Studies of Parameter Identification of Linear and Nonlinear Ship Steering Dynamics*; Report 1920-6; Ministry of Commerce and Industry: Gothenburg, Sweden, 1977.
28. Li, J.Q.; Zhang, G.Q.; Shan, Q.H.; Zhang, W.D. A Novel Cooperative Design for USV-UAV Systems: 3D Mapping Guidance and Adaptive Fuzzy Control. *IEEE Trans. Control. Netw. Syst.* **2023**, *10*, 564–574. [[CrossRef](#)]
29. Zhang, G.Q.; Li, J.Q.; Jin, X.; Liu, X. Robust adaptive neural control for wing sail assisted vehicle via the multiport event-triggered approach. *IEEE Trans. Cybern.* **2022**, *52*, 12916–12928. [[CrossRef](#)]
30. Li, G.S.; Zhang, X.K. Research on the Influence of Wind, Waves, and Tidal Current on Ship Turning Ability Based on Norrbin Model. *Ocean Eng.* **2022**, *259*, 111875. [[CrossRef](#)]
31. Zhang, X.K.; Yang, G.P. Improvement of Nonlinear Norrbin Mathematical Model for Large Ships. *Nav. China* **2016**, *39*, 50–53.
32. Li, G.S.; Zhang, X.K. Green Energy-Saving Robust Control for Ship Course-Keeping System Based on Nonlinear Switching Feedback. *Ocean Eng.* **2023**, *268*, 113462. [[CrossRef](#)]
33. Yang, G.P.; Cheng, W.C.; Zhong, L.; Qiu, Y.M.; Zhang, X.K. Improvement of Nonlinear Norrbin Model for 300,000-Ton Ships. *Ship Sci. Technol.* **2020**, *42*, 35–41.
34. Clarke, D.P.; Gedling, P.; Hine, G. Application of Maneuvering Criteria in Hull Design Using Linear Theory. *Nav. Archit.* **1983**, *11*, 45–68.

Disclaimer/Publisher’s Note: The statements, opinions and data contained in all publications are solely those of the individual author(s) and contributor(s) and not of MDPI and/or the editor(s). MDPI and/or the editor(s) disclaim responsibility for any injury to people or property resulting from any ideas, methods, instructions or products referred to in the content.